The Influence of Coastal Shape on Winter Mesoscale Air–Sea Interaction

DAVID ATLAS AND SHU-HSIEN CHOU

Goddard Laboratory for Atmospheric Sciences, NASA/Goddard Space Flight Center, Greenbelt, MD 20771

WILLIAM P. BYERLY

Systems and Applied Sciences Corporation, MD 20840 and *Goddard Laboratory for Atmospheric Sciences, NASA/Goddard Space Flight Center, Greenbelt, MD 20771*

(Manuscript received 24 March 1982, in final form 9 November 1982)

ABSTRACT

In the case of cold air outbreaks, the combination of the coastal shape and the sea surface temperature (SST) pattern is shown to have a profound effect in establishing a low level mesoscale atmospheric circulation as a result of differential heating due to both variations in overwater path length and the SST. A convergence (or divergence) line then forms along a line exactly downwind of the major bend in the coastline. This is consistent with the structure of the cloud patterns seen in a high resolution Landsat picture of the cloud streets. The major features are also simulated well with a boundary layer model. The dominant convergence line is marked by notably larger clouds. To its east the convective roll clouds grow downstream in accord with the deepening of the boundary layer. To its west (i.e., coastal side) near the convergence line where the induced pressure field forces a strong westerly component in the boundary layer, the wind shear across the inversion gives rise to Kelvin–Helmholtz waves and billow clouds whose orientation is perpendicular to the shear vector and to the major convergence line. The result is a pattern of cloud streets oriented N–S along the wind direction to the east of the convergence line, and billow clouds oriented essentially E–W to the west of that line. It is also suggested that the induced mesoscale circulation will feed back on the ocean by intensifying the wind-generated ocean wave growth and altering their orientation.

1. Introduction

In a previous paper, Chou and Atlas (1982), hereafter referred to as C/A, discuss a satellite-based method of deducing the sensible and latent heating of the atmosphere by the fluxes from the ocean during cold air outbreaks. In that study, we used imagery from both TIROS-N and GOES to observe the so-called "cloud free path" (CFP), the structure and orientation of the cloud streets, and the sea surface temperature (SST) between shore and the cloud edge. In order to deduce the rate of deepening of the convective boundary layer downstream along the flow, we attempted to use the IR cloud top temperatures observed by the TIROS-N Advanced Very High Resolution Radiometer (AVHRR). We found this to be impossible because most of the clouds near the line of initial cloud formation did not fill the 1×1 km field of view of the radiometer. However, we were fortunate to find that Landsat-3 with its 80 m resolution passed over the area of interest off the coast of New Jersey on the day of our study. The accompanying picture, Fig. 1, having dimensions of 180×340 km is a composite of two Landsat frames. The purposes of this paper are to interpret the Landsat cloud picture in terms of the atmospheric mechanisms, to demonstrate that these mesoscale processes resulted from differential heating of the cold land air over the ocean due in large part to the shape of the coast, and finally to show that the induced mesoscale circulation feeds back to affect the ocean.

2. Cloud interpretation and postulates

In addition to showing the primary features seen in the AVHRR photo in Fig. 10 of C/A, namely the main cloud streets oriented N–S in agreement with the surface winds (see Fig. 11 of C/A) and cloud dimensions increasing downwind, consistent with the increasing depth of the mixed layer due to heating from below (see Fig. 3), Fig. 1 shows two other remarkable features which were not clearly discernible in the lower resolution TIROS-N imagery. These are: 1) the line of distinctly larger clouds, indicated as the curve AB, and 2) clouds to the left of the latter curve are distinctly smaller than those to its right and are aligned in a general E–W direction as opposed to the N–S direction on the right. Our purpose is to show that these features are due to the establishment of a mesoscale circulation, and indeed, that the cloud line AB is a mesoscale front across which the low level winds shift sharply. We shall demonstrate how this mesoscale circulation is established and postulate some broader implications.

© 1983 American Meteorological Society

Unauthenticated | Downloaded 06/23/24 07:34 AM UTC

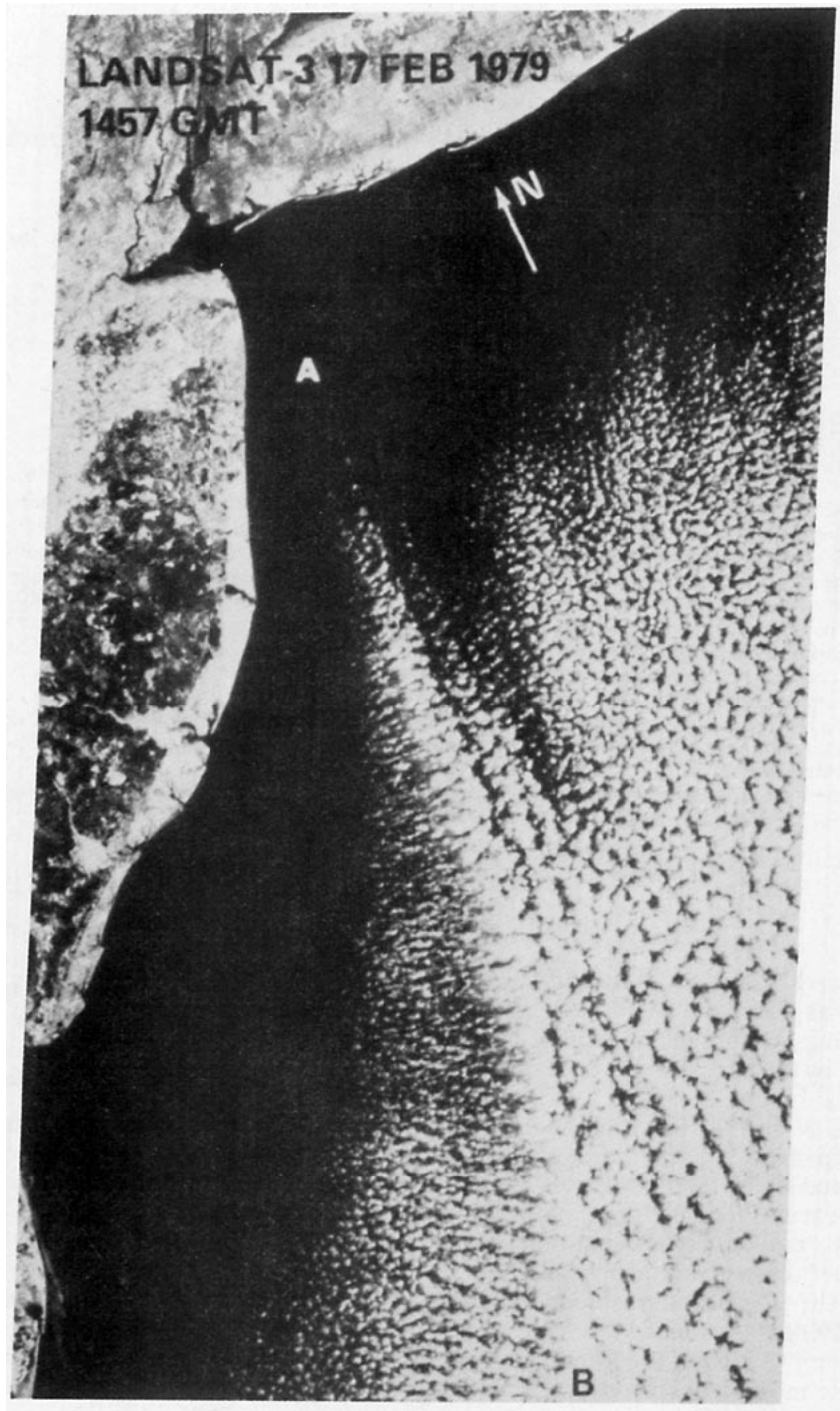

FIG. 1. Cold air outbreak on 17 February 1979 as seen by Landsat-3 visible channel at 1457 GMT. See text for the explanation on the curve AB.

We suggest that the mesoscale circulation comes about in the following way. On this day (17 February 1979) the wind coming off the shore is generally out of the north and is essentially constant in direction along the entire coast of Long Island (NY), and New Jersey. The wind speed is also virtually constant at 10 m s^{-1} over the region as seen at both the shore stations and the buoy about 75 km off the Long Island, NY shore as in Fig. 11 of C/A. The wind speed at the buoy actually varies between 9 and 13 m s^{-1} with a maximum around 0500 EST and a minimum around 1300 EST. The wind direction remains 350°

Unauthenticated | Downloaded 06/23/24 07:34 AM UTC

± 10° all day long. The temperature of the surface air on departing the Long Island and New Jersey coasts is also essentially the same; i.e., −16 to −14.4°C. The major difference in the air on either side of the postulated convergence line AB is thus due to the difference in the path length of overwater travel and the mean temperature of the underlying water surface (see Fig. 2 and the SST map of Fig. 12 in C/A). To the west of the convergence line, the air along any latitude has had both a shorter path over water and a colder path averaged SST than the corresponding points to the east of the line.

The result is that the line AB represents a boundary between warmer air to the east with a relatively deep boundary layer and reduced surface pressures, and the colder air to the west with a shallow boundary layer and relatively high surface pressures. The differences in air temperature, boundary layer height, and surface pressure in an E–W direction across the line AB are such as to cause the low level winds to its west to accelerate to the east, in the manner of a sea breeze front. This is almost certainly the cause of the striking line of convergence and larger cloud elements which comprise the line AB.

To the east of the "front," the clouds are clearly of a convective nature and continue to grow in horizontal dimension downstream, presumably in some proportion to the increasing depth of the boundary layer. Also in the eastern region, the cloud streets are oriented almost identically with the wind direction because of the very large heating rates there and the correspondingly large vertical momentum exchange, which precludes the existence of significant vertical shear.

To the west of the front, however, the clouds are not only smaller and oriented differently, but they are wavelike in character and show no evidence of changing wavelength in the N–S direction. It seems likely that the clouds in the western region are the result of Kelvin–Helmholtz waves whose orientation is perpendicular to the shear vector between the velocity of the mixed layer (i.e., with a NW component) and the strong NNW flow above. Such a shear vector would tend to have a N–S direction and thus give rise to the E–W cloud orientation. While, we have no ocean surface wind data to the west of the convergence line to confirm these explanations, and indeed very little to the east, we believe that the combination of the model results discussed below and the Landsat picture itself provide persuasive evidence in their support. However, substantive proof must await the results of experiments designed to confirm the present hypotheses. Such experiments are now planned.

3. Model results

In order to test the above hypotheses, we have used Stage and Businger's (1981a,b) mixed layer model to compute the boundary layer height (Z_B), surface air temperature (T_0), and surface pressure (P_0) fields. The Stage and Businger model is a Lagrangian model. Assuming a steady state situation as qualified below, we are able to obtain the parameters Z_B, T_0 and P_0 as a function of the downwind distance; i.e., along a straight line running N–S parallel to the "front" AB. Computations were made along 10 such parallel trajectories on both sides of the "front", thus allowing the construction of maps of Z_B, T_0 and P_0. The initial temperature and humidity soundings at the New Jersey and the Long Island shores are assumed to be the same and are identical to those at JFK International Airport, New York at 1200 GMT 17 February 1979. The mean mixed layer wind speed is assumed to be 10 m s^{-1} with the wind blowing from the north and nearly perpendicular to the Long Island shoreline. The divergence is taken to be 1.5×10^{-5} s^{-1} which is estimated from the 700 mb National Meteorological Center (NMC) analysis of vertical velocity assuming constant divergence below. The sea surface temperature (SST) adopted is shown in Fig. 2 and is

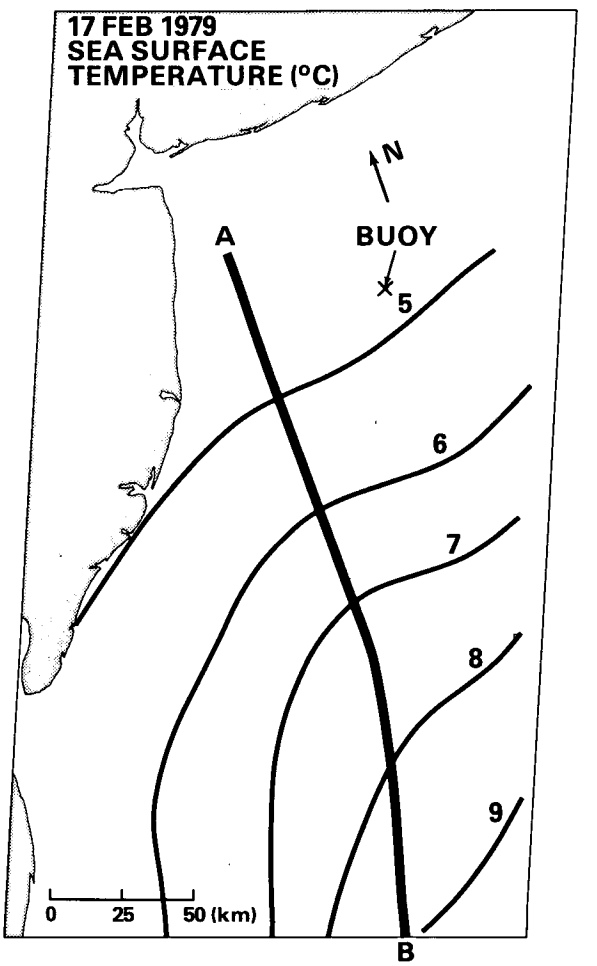

FIG. 2. Weekly mean sea surface temperature for the period 14–21 February 1979.

Unauthenticated | Downloaded 06/23/24 07:34 AM UTC

taken from the map of weekly mean SST (Fig. 12 of C/A). The curve AB in Fig. 2 corresponds to the line of distinctly larger clouds in Fig. 1. It can be seen from Fig. 2 that the northerly air flow is generally across the SST isotherms in the region east of the curve AB, while the air flow is more nearly parallel to the SST isotherms to the west of AB. With a wind speed of 10 m s^{-1}, it takes ~7 h for the air to the east of AB and 3–7 h for that to the west to travel from the shore to the lower end of Fig. 1. Therefore, the clouds of Fig. 1 are associated with air parcels leaving the shore at ~0800–1500 GMT. Within this period, the surface air temperature at the shore fluctuates by ~1.5°C with the minimum temperature at 1200 GMT. At the shore, the surface specific humidity and wind speed are also fairly steady within the same period. Furthermore, the satellite pictures from the GOES-2 visible channel show that the cloud pattern, similar to that in Fig. 1, lasts throughout the daytime period. Therefore, the steady state assumption seems reasonable for the present purposes.

Fig. 3 shows the map of the boundary layer height, surface air temperature and surface pressure generated from the Stage and Businger mixed layer model. Since it turns out that the Z_B and T_0 contours are essentially concentric with the isobars, only the latter are shown in 1-mb steps. However, the corresponding values of Z_B and T_0 are also labeled in Fig. 3. In estimating the surface pressure, it is assumed that the pressure–height relationship above the boundary layer is the same as that of the initial sounding. Therefore, the pressure at the boundary layer top (P_B) can be obtained from this relationship and the computed Z_B. The surface pressure (P_0) can then be estimated by integrating the hydrostatic equation from the boundary layer top (P_B) to the sea surface using the computed temperature and water vapor mixing ratio. We note that the computed pressure pattern reflects only the mesoscale effects because the large scale forcing has been filtered; i.e., we assume no pressure gradient force at the top of the boundary layer. The dashed curves in Fig. 3 indicate the synoptic scale pressure pattern, which is taken from the surface weather map of Fig. 11 of C/A less 4 mb. The reason for adjusting the synoptic scale pressure field is that the surface pressure of the initial sounding at the shore is ~1036 mb (1200 GMT) instead of 1040 mb (1500 GMT) as indicated in the weather map. It can be seen from Fig. 3 that the mesoscale and the synoptic scale pressure patterns are in general agreement, except that the mesoscale field gives more detailed information around the curve AB. Also, the mesoscale N–S pressure gradient is in good agreement with that derived from the shore station at Islip, Long Island, and the buoy ~75 km south (see Fig. 11 of C/A). This amounts to 2.7×10^{-2} mb km^{-1} as compared with 2.5×10^{-2} mb km^{-1} in our calculations. Note that the model generated surface air temperature at the buoy is also in good agreement with the observation, which is ~ −12°C for the period 1200–1600 GMT.

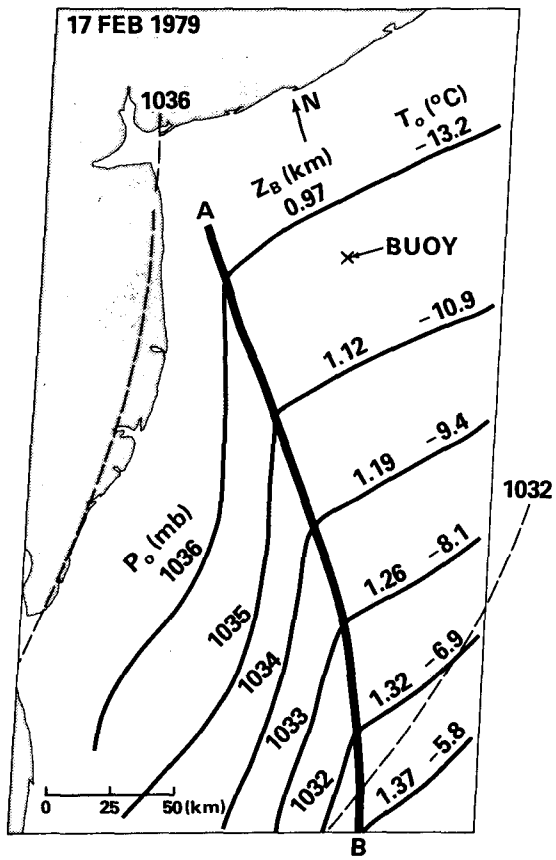

FIG. 3. The boundary layer height (Z_B), the surface air temperature (T_0) and the surface pressure (P_0) generated from Stage and Businger's (1981a,b) mixed layer model (solid curves). The dashed curves correspond to the synoptic scale pressure pattern of Fig. 11 in Chou and Atlas (1982) less 4 mb.

It can be seen from Fig. 3 that the contours of P_0, Z_B and T_0 virtually follow the configuration of the shoreline near the coasts of New Jersey and Long Island. Due to modification from the sea surface, however, the isopleths gradually change downstream to follow the SST isotherms, especially near the lower right corner of Fig. 3. This change occurs mainly on the western side of the "front" because the isobaric pattern is generally parallel to the SST isotherms in the region east of the curve AB. Note that, at each isobar, the SST and the overwater paths are approximately the same for all the N–S trajectories to the east of the curve AB. This results in a simple situation there; i.e., the boundary layer is warming and growing (the surface pressure is dropping) downstream (southward) and the E–W pressure gradient is nearly negligible as compared to that on the western side.

On the other hand, the situation to the west of the curve AB is quite different. There, the air flow is more

Unauthenticated | Downloaded 06/23/24 07:34 AM UTC

nearly parallel to the SST isotherms (which tend to parallel the coast) with the SST increasing eastward. More importantly, the overwater paths from shore also increase eastward. Therefore, the boundary layer height and the surface air temperature increase and the surface pressure decreases downstream and eastward to the curve AB.

The E–W surface pressure gradient is $\sim 3.1 \times 10^{-2}$ mb km^{-1} from the Delaware coast to 20 km west of the curve AB, and increases to 8.7×10^{-2} mb km^{-1} from there to the front. This indicates that the differential heating over the ocean has given rise to the development of a strong mesoscale circulation and that the curve AB does indeed represent a front as originally postulated. We conducted several numerical experiments (not shown) with the mixed layer wind speed equal to 10 m s^{-1}, 20 m s^{-1}, and with wind speeds varying in a manner consistent with the divergence field. These indicated that the computed pressure pattern is insensitive to the mean mixed layer wind speed. This is mainly due to the transfer coefficients of heat through the air–sea interface being independent of wind speed in Stage and Businger's model (see discussion in C/A). If the parameterization of the turbulent transfer coefficients through the air–sea interface is similar to that in Stage and Businger's model, we therefore expect that the model dependency of the resulting pressure pattern will be very small.

In order to make a semi-quantitative estimate of the winds in the boundary layer to the west of the front, we have approximated the solution as follows. The vertically averaged equation of motion may be written as (Lavoie, 1972)

$$dU/dt = fV - \rho^{-1}\partial p/\partial x - C_D U(U^2 + V^2)^{1/2}/(Z_B - h), \quad (1)$$

$$dV/dt = -fU - \rho^{-1}\partial p/\partial y - C_D V(U^2 + V^2)^{1/2}/(Z_B - h), \quad (2)$$

where (x, y) is the traditional Cartesian coordinate system with the origin fixed at the Delaware coast, i.e., $\sim$38.5°N, 75°W, t time, U and V the x and y components of the mean boundary layer velocity, respectively, ρ density, p pressure, f the Coriolis parameter, C_D drag coefficient, and Z_B and h the heights of the mixed layer and the surface boundary layers, respectively. The value of h is generally much smaller than that of Z_B. In the Stage and Businger mixed layer model, h is assumed to be negligible as compared to Z_B, but the effects of the unstable surface boundary layer (i.e., where the temperature profile is superadiabatic) on the mixed layer growth are included through the parameterization of the fluxes of momentum, heat and moisture at the air–sea interface. Note that the values of Z_B and h are not needed for the following analysis. If we assume $dV/dt = 0$ and $dU/dt \approx U\partial U/\partial x$, then (1) and (2) can be combined into

$$U\partial U/\partial x = fV + fU^2/V - \rho^{-1}\partial p/\partial x + \rho^{-1}\partial p/\partial y(U/V). \quad (3)$$

For the region around 38.5°N ($y = 0$) and between the Delaware coast and the curve AB, the y component of the mean surface pressure gradient is $\sim 2.5 \times 10^{-2}$ mb km^{-1}. The x component of the surface pressure gradient is $\sim 3.1 \times 10^{-2}$ and 8.7×10^{-2} mb km^{-1}, respectively, for $x = 0$–100 km and $x = 100$–120 km. The front is located at $x = 120$ km. The average pressure gradient for the mixed layer is taken to be half that at the surface, because the pressure gradient is zero at the top of the mixed layer. If $V = -10$ m s^{-1} (uniform northerly wind), then (3) implies that the mesoscale pressure pattern can generate a westerly wind component of ~ 4 m s^{-1} at $x = 100$ km with $U = 0$ near the shore ($x = 0$) and $U = 9$ m s^{-1} near the mesoscale front along AB ($x = 120$ km). The induced westerly wind component near the front is therefore significant, again demonstrating the curve AB to be a convergence line similar to a sea breeze front.

We note that the above analysis is very simple, it is intended only to provide semi-quantitative support for the ideas that the curve AB is a mesoscale convergence line and that the clouds on its west are due to Kelvin–Helmholtz (K–H) instability. A more complete solution will probably require a three-dimensional model including the effects of roll vorticities in the PBL.

4. The cloud streets

We now discuss the nature of the cloud streets on either side of the front in the light of the model results. The mean flow pattern of the boundary layer in the region west of the curve AB may be deduced from the above analysis. Combining the general northerly flow with the westerly flow induced by the mesoscale pressure pattern, the flow pattern tends to have a northerly wind initially (i.e., near the New Jersey shore) which gradually turns into a NW flow when approaching the curve AB. Assuming a 300 m depth for the inversion layer and adopting the model calculated boundary layer height, the wind at the top of the inversion layer taken from the wind profiles at JFK International Airport, New York and Wallops Island, Virginia is ~ 22 m s^{-1} with NNW flow. This wind and that deduced in the boundary layer near the front suggest a N–S vertical wind shear across the inversion layer. Because of the paucity of data and the nature of the assumptions we were reluctant to compute either the modified sounding or the magnitude of the shear in order to estimate the Richard-

Unauthenticated | Downloaded 06/23/24 07:34 AM UTC

son number Ri. However, the combination of thermal stability and shear across the inversion are the ingredients required to produce small Ri and K–H instability. We therefore postulate that the clouds to the west of the front are very probably K–H billows with their orientation normal to the N–S wind shear vector (Brown, 1980) and thus essentially perpendicular to the front.

Kelvin–Helmholtz instability is a form of dynamic instability which occurs within a hydrostatically stable layer with strong vertical shear in the velocity profile. A necessary condition for the occurrence of K–H instability is that the local gradient Richardson number should be less than 0.25 (Miles and Howard, 1964). For the most unstable wave, the relationship between the wavelength (λ) and the thickness of the dynamically unstable shear layer (ΔZ) suggested by Miles and Howard (1964), and Woods (1969) is $\lambda = 7.5\Delta Z$ and that by Scorer (1969) is $\lambda = 4\pi\Delta Z$.

Fig. 4 shows the roll wavelength (λ) and the aspect ratio (λ/Z_B) versus distance downwind from the Long Island shore for the regions ~30 km east and west of the curve AB, respectively. The wavelength is visually estimated from the Landsat picture and the boundary layer height is taken from the model results. In the eastern region, the wavelength is ~3–10 km and the aspect ratio is ~3–7. These are in good agreement with the findings of Kuettner (1971), and LeMone (1973). Both the wavelength and the aspect ratio increase downstream with larger increases beyond 150 km of over water travel. This result, together with the fact that the cloud street orientation is ~20° to the left of the surface geostrophic wind (parallel to the mean wind in the boundary layer) suggests that the cloud streets to the east of the front are convective roll clouds in the boundary layer, which are caused by convective instability and the inflectional point instability as discussed by Kuettner (1971), Brown (1970, 1972), LeMone (1973), Lilly (1966), and others.

In the western region, on the other hand, the wavelength and the aspect ratio are virtually independent of fetch and are ~3 km and 3, respectively. Moreover, the wavelength appears to be independent of boundary layer height. This is also in agreement with the K–H instability theory that the most unstable wavelength is related to the thickness of the dynamically unstable shear layer (i.e., the inversion) and not to the boundary layer beneath it. The thickness of the inversion layer estimated from the aforementioned λ–ΔZ relations is in the range of 240–400 m if λ = 3 km, not an unreasonable result. As noted earlier, the clouds to the west of the front clearly have a wave-like character with their long dimension very much larger than their short dimension. All of the above provides strong circumstantial evidence that these clouds are very probably K–H billow clouds as suggested earlier. We await more direct experimental evidence to prove this point.

5. Impact on ocean waves

At least one other significant result may be deduced from the present findings. This relates to the feedback of the induced mesoscale circulation on the generation of ocean waves. Our associates in the Instrument Systems Division of this Center have been flying a sophisticated surface contour radar system to detect,

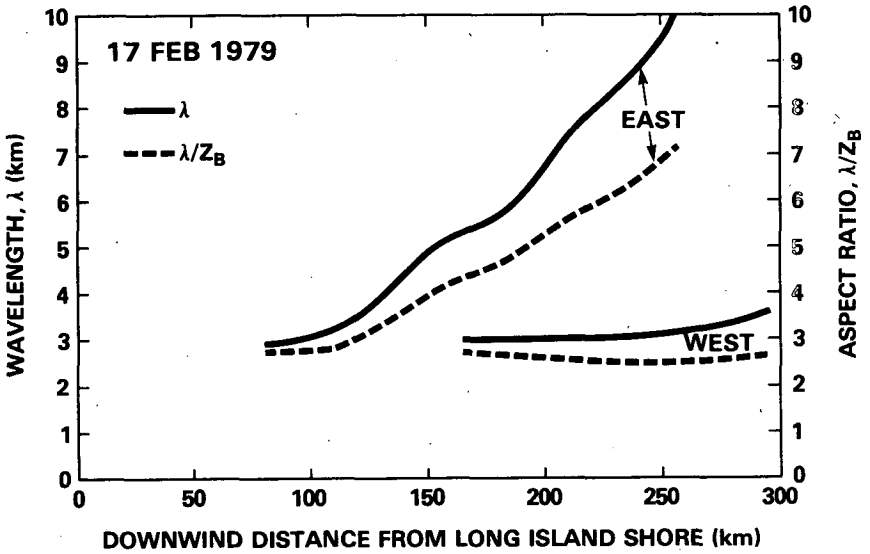

FIG. 4. Roll wavelength (λ) and aspect ratio (λ/Z_B) versus the distance downwind from the Long Island shore for the regions ~30 km east and west of the mesoscale front. Wavelength (λ) is estimated from the Landsat picture and the boundary layer height (Z_B) is taken from the results of Stage and Businger's (1981a,b) mixed layer model.

Unauthenticated | Downloaded 06/23/24 07:34 AM UTC

measure and display the structure and amplitude of ocean waves with a vertical resolution of 15 cm. The data from a swath some 500 m wide and 4–5 km in length is summarized in a two-dimensional Fourier analysis of the directional ocean wave spectra. Successive spectra for each segment along the flight path document the downwind evolution of the waves (Kenney, *et al.*, 1979).

In order to study the development of fetch-limited waves, they have been flying on days of cold air outbreaks when the winds are strong and unidirectional in the hope of finding the simplest possible wave structure and determine the growth of wave amplitude and energy. Dr. Edward Walsh (private communication, 1981) reports that even in these supposedly simple situations, in addition to the expected wave orientation perpendicular to the wind direction, there appears an unexplained secondary peak at another direction at distances of some 100 km off shore.

We suggest that the occurrence of such bimodal directional wave spectra on days when the synoptic scale surface flow is unidirectional may be attributable to the mesoscale windfield induced in the manner previously described. In the case shown, we have deduced the development of NNW to NW surface winds (near the front) to the west of the mesoscale front in addition to the enhancement of the basic northerly flow to the east of that front. The waves generated by each of these winds will obviously travel across the frontal position so that in some swath of presently unknown dimensions centered along the front, one will find both wave directions in the spectra. In the case shown in Fig. 3, we expect the dominant waves to be oriented essentially E–W to the east of the front and to reach their peak amplitude along the front where the N–S fetch is bounded. On the south and west side of the front the latter waves will decay with distance from the front. Similarly, the NE–SW oriented waves generated by the induced NNW and NW winds to the west of the front will reach their peak amplitude at the front and decay with increasing distance to its east. The result is that the front represents the locus along which one will find both wave directions at their peak amplitude.

Unfortunately, Walsh did not fly in a situation identical to the present one, nor does he have sufficient data to verify the above explanation. Thus, while this explanation seems entirely reasonable, it must be considered as a hypothesis to be tested in future flights. At the time of this writing Walsh believes that the second peak in his directional wave spectrum is due to swell and not to the process described here.

6. Summary and conclusions

In cases of cold air outbreaks, we have shown that the combination of the shape of the coast and the sea surface isotherms can have a profound effect in establishing a mesoscale atmospheric circulation as a result of differential heating due to both variations in overwater path length and the underlying SST. When the coastal effects dominate, a mesoscale front forms downstream of the point marking the major bend in the orientation of the coastline. Moreover, the sea level isobars tend to parallel the shape of the coast, but pressure will always decrease with distance from shore as the boundary layer air is progressively warmed. Thus, when the coastline is concave towards the downwind direction a mesoscale low will form, and the converse occurs when the coast is convex toward that direction.

The strength of the induced mesoscale circulation obviously depends upon the original contrast between the land air temperature and the SST. In any case, the mesoscale circulation and enhanced winds will in the first instance, feed back on the ocean by intensifying the wave growth and altering their directions. This is one of the possible reasons for the observation of bidirectional ocean wave spectra when the synoptic scale flow is unidirectional. The induced pattern of sea–surface stress is also bound to have an additional effect on the coastal oceanic circulation, but this has not been discussed in the present paper.

It is worth noting that where the coastline and the isotherm pattern are more or less normal to the mean flow in the boundary layer, and the thermal contrast is sufficiently large, the cloud streets formed downstream will be convective in nature and oriented with the axes of roll vortices along the wind direction. The convective elements will also grow three dimensionally in the downwind direction in approximate proportion to the depth of the boundary layer.

On the other hand, where the mean wind in the boundary layer is nearly parallel to the coastline and the SST isotherm pattern and the sea level isobars tend to parallel the coastline as noted earlier, one will establish a significant vertical wind shear across the inversion at the top of the boundary layer. The combination of the thermal stability and strong shear in this region is thus likely to give rise to Kelvin–Helmholtz waves and billow clouds such as we have interpreted to be present in the Landsat picture of Fig. 1.

Although the above analysis appears persuasive, we recognize that much of it is based upon circumstantial evidence rather than direct observation. We therefore recommend a carefully designed field experiment to validate our interpretations.

Finally, we note that almost none of the above interpretations would have been possible without the high resolution Landsat pictures. We believe that an understanding of many such physical processes will emerge from the detailed study of such high resolution imagery and recommend that meteorologists and oceanographers exploit them fully.

Unauthenticated | Downloaded 06/23/24 07:34 AM UTC

Acknowledgments. We are grateful for enlightening discussions with many of our colleagues in Goddard Laboratory for Atmospheric Sciences (GLAS), most particularly Dr. Robert Atlas, Dr. Eugenia Kalnay, Dr. Milton Halem, Dr. Joanne Simpson, Dr. D. B. Rao, Dr. Michael C. McCumber, and Dr. Paul Schopf. We also appreciate the general assistance of Mr. Earl Kreins and William C. Skillman and the fine typing and editorial work of Mrs. Sharon Anderson.

REFERENCES

Brown, R. A., 1970: A secondary flow model for the planetary boundary layer. *J. Atmos. Sci.*, **27**, 742–757.

——, 1972: On the inflection point instability of a stratified Ekman boundary layer. *J. Atmos. Sci.*, **29**, 850–859.

——, 1980: Longitudinal instabilities and secondary flows in the planetary boundary layer: A review. *Rev. Geophys. Space Phys.*, **18**, 683–697.

Chou, S. H., and D. Atlas, 1982: Satellite estimates of ocean–air heat fluxes during cold air outbreaks. *Mon. Wea. Rev.*, **110**, 1434–1450.

Kenney, J. E., E. A. Uliana and E. J. Walsh, 1979: The surface contour radar, a unique remote sensing instrument. *IEEE Trans., Microwave Theory Tech.*, **27**, 1080–1092.

Kuettner, J. P., 1971: Cloud bands in the earth's atmosphere: Observations and theory. *Tellus*, **23**, 404–426.

Lavoie, R. L., 1972: A mesoscale numerical model of lake-effect storms. *J. Atmos. Sci.*, **29**, 1025–1040.

LeMone, M. A., 1973: The structure and dynamics of horizontal roll vortices in the planetary boundary layer. *J. Atmos. Sci.*, **30**, 1077–1091.

Lilly, D. K., 1966: On the instability of Ekman boundary flow. *J. Atmos. Sci.*, **23**, 481–494.

Miles, J. W., and L. N. Howard, 1964: Note on a heterogeneous shear flow. *J. Fluid Mech.*, **20**, 331–336.

Scorer, R. S., 1969: Billow mechanics. *Radio Sci.*, **4**, 1299–1307.

Stage, S. A., and J. A. Businger, 1981a: A model for entrainment into a cloud-topped marine boundary layer. Part I: Model description and application to a cold air outbreak episode. *J. Atmos. Sci.*, **38**, 2213–2229.

——, and ——, 1981b: A model for entrainment into a cloud-topped marine boundary layer. Part II: Discussion of model behavior and comparison with other models. *J. Atmos. Sci.*, **38**, 2230–2242.

Woods, J. D., 1969: On Richardson's number as a criterion for laminar–turbulent–laminar transition in the ocean and atmosphere. *Radio Sci.*, **4**, 1289–1298.

Unauthenticated | Downloaded 06/23/24 07:34 AM UTC